



COMBINED PHOTOVOLTAIC AND SOLAR THERMAL SYSTEMS FOR FACADE INTEGRATION AND BUILDING INSULATION

STEFAN KRAUTER^{*†}, RODRIGO GUIDO ARAÚJO*, SANDRA SCHROER*,
ROLF HANITSCH**, MOHAMMED J. SALHI***, CLEMENS TRIEBEL*** and
REINER LEMOINE***

*Laboratório Fotovoltaico, Coordenação do Programa de Pós-graduação de Engenharia da Universidade Federal do Rio de Janeiro, UFRJ-COPPE/EE, Caixa Postal 68504, Rio de Janeiro, 21945-970 RJ, Brazil

**Institute for Electrical Energy Systems, Berlin Institute of Technology, Sec. EM 4, Einsteinufer 11, D-10587 Berlin, Germany

***SOLON AG für Solartechnik, Schlesische Strasse 27, D-10997 Berlin, Germany

Received 2 September 1999; revised version accepted 9 April 2000

Communicated by BRIAN NORTON

Abstract—Most photovoltaic (PV) facades are built as curtain facades in front of thermally insulated buildings, with air ducts in between. This causes additional costs for support structure and installation, while heat dissipation from the solar cells is often not optimal. Measurements carried out are facing both concerns: integration of a thermal insulating layer (which meets the latest German heat-preserving regulation, WSV 95) into the PV facade, plus additional cooling by active ventilation or water flow. Active ventilation at conventional curtain PV facades allows a reduction of cell operating temperatures of 18 K, resulting in an 8% increase in electrical energy output at an airspeed of about 2 m/s. Cell temperatures increase by 20.7 K at thermal insulating PV facade elements (TIPVE) without cooling, which causes a 9.3% loss of electrical yield, but installation costs can be reduced by 20% (all related to a conventional PV curtain plus a heat-insulating facade at a building). HYTIPVE, a hybrid thermal insulating PV facade element combined with a water cooling system, which could also serve for heating up water, lowers the operating cell temperature by 20 K and increases electrical yield by 9% (compared with conventional curtain PV facades). Further economic investigations of such a HYTIPVE, including its operational costs and substitution effect, related to the electrical and thermal yield, are in progress. © 2000 Elsevier Science Ltd. All rights reserved.

1. INTRODUCTION

The application of solar energy technology to buildings often depends on its ability to be integrated into common building structures, such as facade elements. Costs of planning, manufacturing and installation may be reduced if components such as substrate, weather protection, photovoltaic (PV) generator, solar thermal collector, thermal insulation and mounting elements could be combined. In particular, the thermal behavior of the PV generator has been investigated for different configurations of the facade structure.

Increased cell temperatures of PV modules lower the power output of typical crystalline silicon PV power plants by -0.3 to -0.5% K^{-1} (Emery *et al.*, 1996; King and Eckert, 1996; Wilshaw *et al.*, 1996). Therefore, as electrical-

yield losses at high operating cell temperatures may be considerable, simulation and control of heat transfer is important. Although good heat transfer (passive or even active) is preferable, installation and mounting costs also have to be taken into consideration for PV facades. Four different kinds of PV facades, i.e., passively and actively cooled, and in combination with an integrated thermal insulation for the building, have been investigated. One part of the investigation (forced backside convection by fans) was carried out at a test facility of the 'Laboratorio Fotovoltaico' at 'Universidade Federal do Rio de Janeiro'; further testing took place at SOLON AG, Berlin. Earlier work predicts a reduction of the cell operating temperature of 3–4 K only for passive cooling by natural convection on the backside of the facade. Other authors mention higher values (Hänel and Imamura, 1992; Posansky and Gnos, 1994; Bendel *et al.*, 1997; Brinkworth *et al.*, 1997; Nordmann *et al.*, 1998; Crick *et al.*, 1997; Crick *et al.*, 1998; Sandberg and Moshfegh, 1998). For the most part, literature

[†]Author to whom correspondence should be addressed. Tel.: +55-21-562-8032, fax: +55-21-290-6626; e-mail: krauter@coe.ufjf.br

reports on thermal performance of certain given facades, making it difficult to compare results. The following investigation has been undertaken to achieve more accurate results in a direct comparison of four very different thermal layouts under static conditions. This was carried out as a prerequisite for an economic evaluation of a new combined facade element that serves as a building insulation, generates electrical power at a high photovoltaic conversion efficiency and allows the use of solar thermal energy as well.

2. MEASUREMENTS

2.1. Test conditions and equipment

The SOLON PV modules ($1220 \times 560 \times 35$ mm) used in the studies consist of 36 multicrystalline silicon solar cells (edge of 125 mm) and have an output power of 68 W under Standard Test Conditions (cell temperature of 25°C , irradiance of 1000 W m^{-2} , and a spectrum equivalent to AM 1.5), see Table 1 and Fig. 1. The ‘artificial wall’ to which the PV modules were mounted (experiments described in Sections 2.2, 2.4, 2.5) was made of smoothed pressboard (2 m wide, 2 m in height and 20 mm thick). The hall in which the experiments were carried out was 32 m by 16 m, with a height of 6 m, and had a white plaster inner surface.

The sun simulator was a ‘steady-state-simulator’, according to the spectral specifications of a ‘Class B’ simulator, and used tungsten-halogen lamps of the type ‘Powerstar HQI-T 2000W/D/I’, by Osram, Berlin. The configuration of the solar simulator is shown in Fig. 2. The spectrum of the lamps is plotted in Fig. 3, as is the AM 1.5 standard spectrum. Taking into account the decrease in average intensity due to the tilt angle of facades, an irradiance level of 700 W m^{-2} is adequate. The actual average irradiance achieved was 702 W m^{-2} , with a maximum of 749 W m^{-2} and a minimum of 655 W m^{-2} . Homogeneity of irradiance on the plane of the module was $\pm 6.7\%$; the distribution is given in Fig. 4.

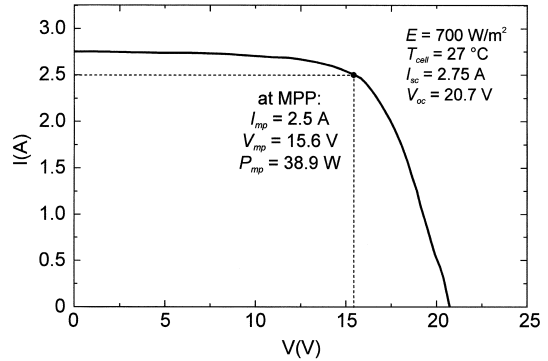


Fig. 1. Current–voltage characteristics of the PV modules used during the experiments.

The PV facade elements were always operated at the maximum power point. Temperature measurements (ambient temperature, as well as upper and bottom back of the PV module temperatures) were made using Pt 100 temperature sensors at 1-min intervals until temperatures reached stationary values (see Figs. 5–9).

2.2. Passively ventilated PV facade element

In the first experimental arrangement, representing a conventional PV curtain facade, a variable air duct was placed between the facade and the wall. Fig. 5 shows the test set-up of this passively ventilated PV facade.

The frame of the PV module was removed, to allow undisturbed natural convection in the air duct behind the module. The frameless module was 6 mm thick, 1205 mm long and 545 mm wide. To avoid disturbances of the convective airflow from the sides, a side cover was attached on both sides of the facade element.

Pt 100 temperature sensors were attached to the rear of the PV module, 230 mm away from the edges and centered. Table 2 shows the stationary temperatures for $t > 30$ min (average duration of measurements). Irradiance was 700 W m^{-2} on the plane of the facade, as determined by the solar simulator described above.

While the effect of the variation of the air duct is only 2.6 K (see Table 2), it could be neglected in terms of output power in the observed range.

Table 1. Nominal electrical data of the PV modules used (at standard test conditions)

Parameter	Values of Solon alpha PV module
Power at MPP under STC P_{mpp}	68 W
Open circuit voltage V_{oc}	21.2 V
Short circuit current I_{sc}	4.42 A
Temperature coefficients TC_V, TC_C, TC_P	$-77 \text{ mV/K}; 1.5 \text{ mA/K}; -0.35 \text{ W/K}$
Maximum Power Point $V_{\text{mpp}}, I_{\text{mpp}}$	17.3 V, 3.93 A

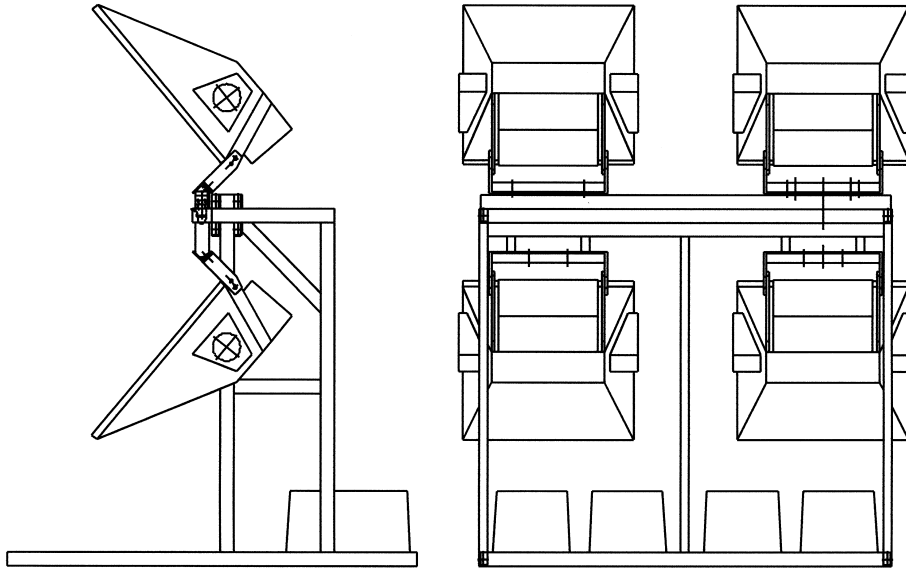


Fig. 2. Configuration of the solar simulator used in the experiments.

2.3. Actively ventilated PV facade element

These measurements were carried out by the ‘Laboratorio Fotovoltaico’ at ‘Universidade Federal do Rio de Janeiro (UFRJ)’. In order to minimize the dispersion of airspeeds along the width of the PV-facade, an array of 16 fans was used. The aim of this experiment was to evaluate the maximum possible effect of active ventilation. Therefore, the front- and back of the PV module were both ventilated, and the module was mounted with its long side towards horizontal (see Fig. 6). The air velocities (measured at the front of the module, 40 mm above the module’s surface) shown in column A of Table 3 allowed a reduction of cell temperature of 16 K, relative to natural convection. This resulted in an increase of 7.2% in output power.

A further experiment (column B of Table 3) was carried out with the same configuration, but an increased air velocity (about 50% more), which

resulted in a reduction of 18 K in the temperature and a power gain of 8.1% (both related to natural convection). If active ventilation could be implemented inexpensively, an appreciable decline in power generation costs would be experienced.

2.4. Thermal insulating PV-facade element (TIPVE)

Thermal insulation (12.5 cm layer of mineral wool) was attached directly to the back of the PV-facade in order to achieve a thermal insulation of $k = 0.32 \text{ W K}^{-1} \text{ m}^{-2}$, in accordance with WSV 95 (Heat Preserving Regulation for Building Materials by the German Government, 1995). This allows the substitution of the insulation layer of the building wall. Fig. 7 shows the test arrangement (temperature measurement configuration was the same as that used for the conventional PV facade element, as shown in Fig. 5).

As can be seen by comparison of Table 4 with

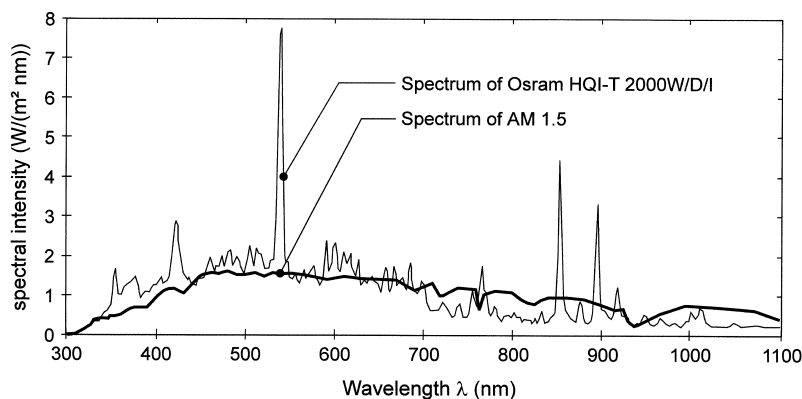


Fig. 3. Spectrum of the solar simulator used in the experiments, in comparison to AM 1.5.

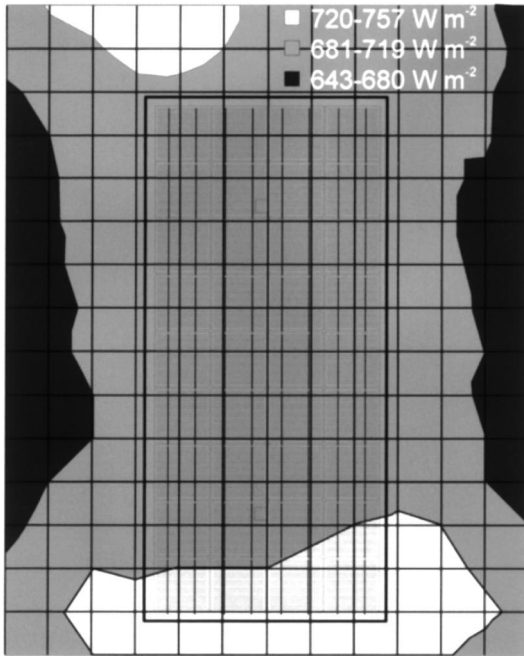


Fig. 4. Homogeneity of irradiance in the plane of the PV modules.

Table 2, cell temperatures at the TIPVE are about 20 K higher than at a conventional PV facade element, which results in a 9% loss of electrical power output, while the TIPVE will lower the

building-equipment costs compared to a conventional arrangement, including a thermal insulated wall plus a curtain PV-facade with an air duct.

2.5. Hybrid thermal insulating PV facade (HYTIPVE)

The most recent development is a thermal insulating PV facade along with an integrated cooling system that consists of a propylene mat and a small water pump (see Fig. 8). The heated water could also be used for thermal applications (directly or combined with solar thermal systems). A model of such PV thermal systems has been presented by Bergende and Løvvik (1996). Table 5 shows the measured stationary temperatures at different flow speeds while using an inlet water temperature of 13.6–15.8°C (water inlet temperature was constant during each experiment). HYTIPVE offers an additional cooling effect of about 20 K compared to conventional PV curtain facades, and is in the same range as that found for active ventilated structures (max. 18 K).

3. SUMMARY & DISCUSSION

Fig. 9 shows the thermal response to the different types of PV facades irradiated at 700 W

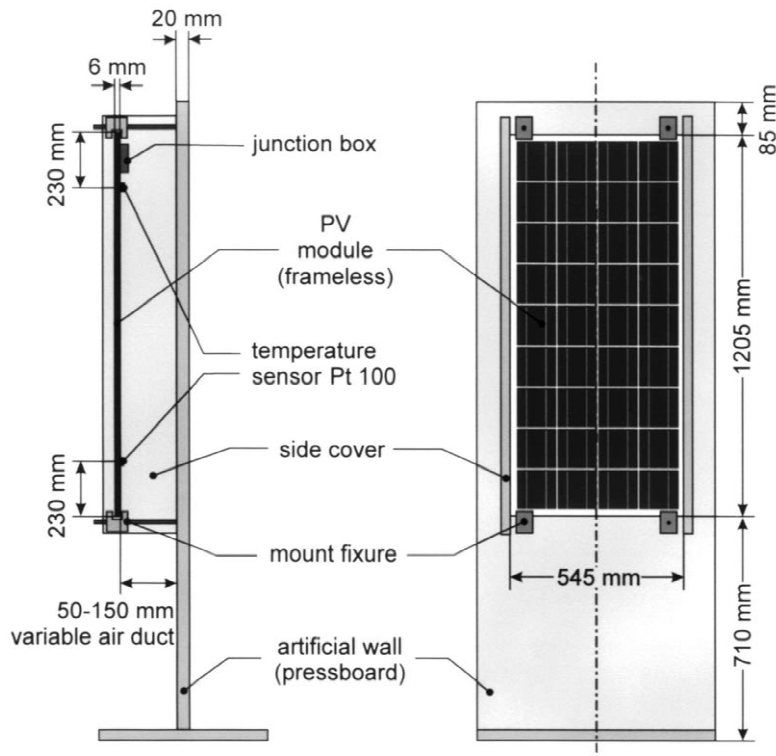


Fig. 5. Side- and front view of the passively ventilated PV facade element (curtain facade).

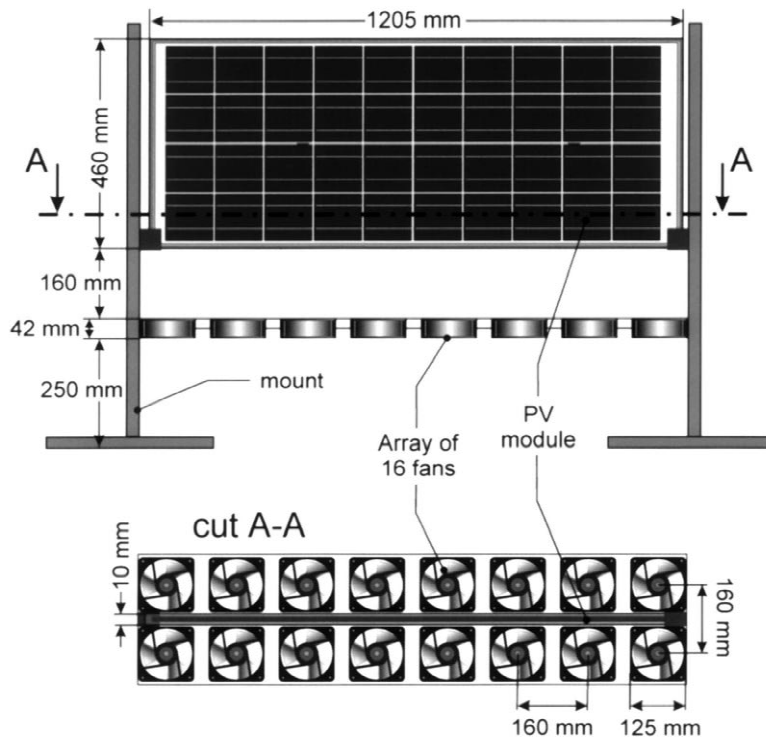


Fig. 6. Side- and top view of the actively ventilated PV module.

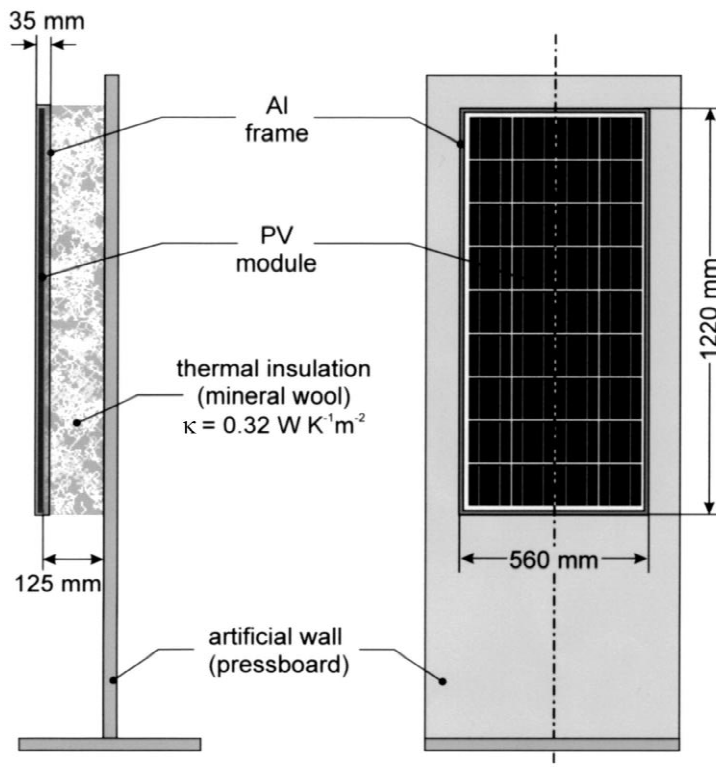


Fig. 7. Side- and front view of the thermal insulating PV facade element (TIPVE).

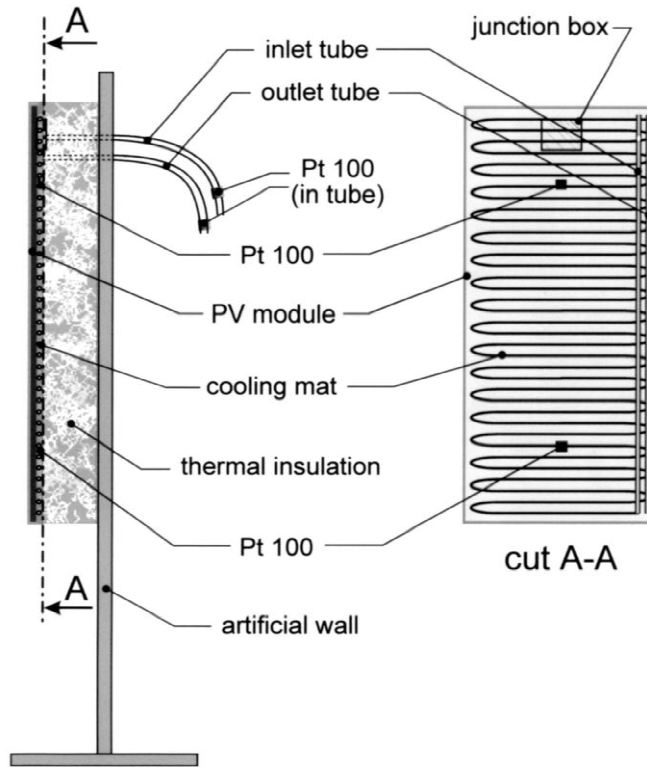


Fig. 8. Side- and rear view of the hybrid thermal insulating PV facade element (HYTIPVE).

m^{-2} for 4 h. Stationary values are reached after one to 2 h.

Table 6 offers an overview of the different measurements, and the consequences on yield and costs:

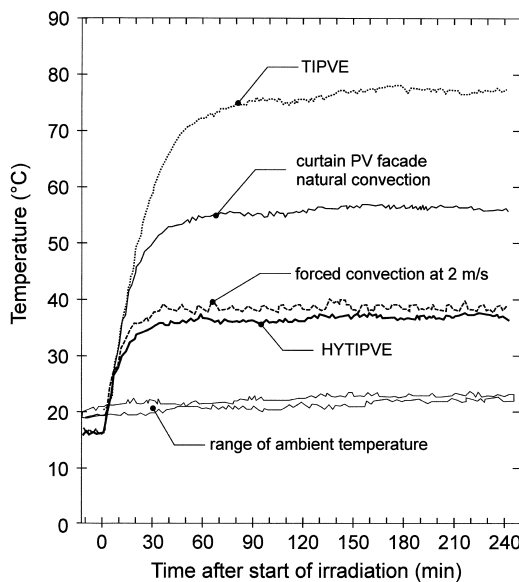


Fig. 9. Temperature as a function of time for different PV facade configurations ($G=700 \text{ W m}^{-2}$).

- Active ventilation by forced convection of 2 m s^{-1} results in a maximum reduction of operating cell temperatures of 18 K. This leads to an 8% increase in the electrical power output in comparison to conventional PV facades.
- Thermal insulating PV facade elements (TIPVE), with $k = 0.32 \text{ W K}^{-1} \text{ m}^{-1}$, lead to a temperature increase of 20.7 K, which causes a 9.3% loss of electrical yield (related to conventional PV curtain facades). Depending on the value of the PV generated electricity in relation to the possible savings of installation costs, such a solution may become an attractive option.
- Hybrid thermal insulating PV facade elements (HYTIPVE), combined with water cooling systems (which may also be used for hot water applications), allow an electrical yield that is 9% higher than that found for conventional PV-facades.

In order to facilitate further investigation, allowing calculation of cell temperatures, efficiencies and energy yields, the theoretical background of the experiments is given in the appendix.

Economic investigations concerning the invested and operational costs of additional com-

Table 2. Comparison of stationary temperatures at a passively ventilated PV facade element

Width of air duct (mm)	T_{cell} (°C)	$T_{\text{upper}} - T_{\text{lower}}$ (K)	T_a (°C)	ΔT_{cell} related to an air duct of 150 mm for $T_a = 20^\circ\text{C}$ (K)
50	56.3	7.4	20.1	2.6
100	57.4	6.4	22.0	1.7
150	55.9	4.7	22.2	0

 Table 3. Distribution of forced convection air velocity, v , in m s^{-1} at the front of a PV-facade element (40 mm above the module's surface)

v (m s^{-1}) Probe	Edge of PV-facade		Center of PV-facade	
	A	B	A	B
Upper	0.8–1.1	1.5–1.8	1.2–1.5	2.0–2.2
Center	0.9–1.1	1.8–2.0	1.4–1.7	2.3–2.5
Lower	1.3–1.5	2.1–2.4	1.5–1.7	2.4–2.6

Table 4. Average values of cell- and ambient temperatures at thermally insulating PV-facades

T_{upper}	T_{lower}	$T_{\text{upper}} - T_{\text{lower}}$	T_a	T_{center}
82.2°C	72.1°C	10.1 K	22.8°C	77.2°C

ponents (such as fans, water pumps, insulation material, installation and substitutive effects) relating to the yield are in progress.

NOMENCLATURE

A	Area (m^2)
AM	Relative air mass
c	Specific heat ($\text{J kg}^{-1} \text{K}^{-1}$)
d	depth of air duct (m)

E	Irradiance (W m^{-2})
G	Global irradiance (W m^{-2})
Gr	Grashof number (–)
g	Standard gravitational acceleration (9.8067 m s^{-2})
h	Heat transfer coefficient ($\text{W m}^{-2} \text{K}^{-1}$)
HYTIPVE	Hybrid thermal insulating PV facade element
I	Electrical current (A)
I_{mpp}	Current at maximum power point (A)
I_{sc}	Short circuit current (A)
k	Thermal conductivity ($\text{W m}^{-1} \text{K}^{-1}$)
l	Length relevant for heat transfer (m)
m	Mass (kg)
\dot{m}	Mass flow (kg s^{-1})
MPP	Maximum power point
Nu	Nusselt number
P	Electrical power (W)
P_{mpp}	Electrical power at maximum power point (W)
Pr	Prandtl number (–)
PV	Photovoltaic
PVE	Photovoltaic facade element
Pt 100	Electrical resistor made of platinum and used for temperature measurements (100 Ohms at 0°C)
q	Heat flux (W m^{-2})
Ra	Raleigh number (–)
Re	Reynolds number (–)
Si	Silicon
STC	Standard test conditions (irradiance of 1000 W m^{-2} at a spectrum equivalent to an air mass of AM 1.5 and a solar cell temperature of 25°C)
t	Time (s)
T	Temperature ($^\circ\text{C}$, K)
T_{cell}	Solar cell temperature ($^\circ\text{C}$, K)

Table 5. Temperatures of a hybrid thermal insulating PV-facade element (HYTIPVE)

Flow rate in $10^{-6} \text{ m}^3 \text{ s}^{-1}$	37	43	47.7
T_{cell} in $^\circ\text{C}$	37.6	39.7	36.8
T_a in $^\circ\text{C}$	22.2	24.0	23.1
ΔT_{cell} in K, related to flow rate of $47.7 \cdot 10^{-6} \text{ m}^3 \text{ s}^{-1}$ (ref. to $T_a = 20^\circ\text{C}$)	2.2	1.9	0
T_{inlet} in $^\circ\text{C}$	13.6	15.8	12.6
T_{outlet} in $^\circ\text{C}$	15.4	17.1	13.9

Table 6. Measurements of stationary temperatures for different types of PV-facade elements (PVE)

	HYTIPVE flow rate of $47.7 \cdot 10^{-6} \text{ m}^3/\text{s}$	PVE ventilated at 2 m/s	conv. PVE- air duct of 150 mm	TIPVE insulation of 125 mm
T_{cell} in $^\circ\text{C}$	36.8	39.6	55.9	77.1
T_a in $^\circ\text{C}$	23.1	24	22.2	22.8
ΔT_{cell} vs. conventional PV-facade, in K (ref. to $T_a = 20^\circ\text{C}$)	–19.9	–18	0	20.7
Gain of electrical yield	9.0%	8.1%	0%	–9.3%
Relative expenditure related to conv. PV-facade (new building)	1.2–1.4	1.1–1.2	1.0	0.8–0.9

T_{center}	Backside temperature at the center of the PV module ($^{\circ}\text{C}$, K)
T_{inlet}	Temperature of water inlet ($^{\circ}\text{C}$, K)
T_{lower}	Backside temperature at the lower part of the PV module ($^{\circ}\text{C}$, K)
T_{outlet}	Temperature of the water outlet ($^{\circ}\text{C}$, K)
T_{upper}	Backside temperature at the upper part of the PV module ($^{\circ}\text{C}$, K)
TC_V	Temperature coefficient of voltage dV/dT (V K^{-1})
TC_I	Temperature coefficient of current dI/dT (A K^{-1})
TC_P	Temperature coefficient of power dP/dT (W K^{-1})
TIPVE	Thermal Insulating PV facade Element
v	Air velocity (m s^{-1})
V	Voltage (V)
V_{mpp}	Voltage at maximum power point (V)
V_{oc}	Open circuit voltage (V)
\dot{V}	Volume flow ($\text{m}^3 \text{s}^{-1}$)
WSW 95	German Heat Preserving Edict of the year 1995 ('Wärmeschutzverordnung, 1995')

Greek letters

β	Thermal expansion coefficient (K^{-1})
ΔT_{cell}	Difference of cell temperature related to reference conditions (K)
η_{PV}	Efficiency of photovoltaic energy conversion (-)
ε	Thermal emittance (-)
λ	Wavelength (m)
ν	Cinematic viscosity ($\text{m}^2 \text{s}^{-2}$)
μ	Dynamic viscosity ($\text{kg m}^{-1} \text{s}^{-1} = \text{N m}^{-2} \text{s}^{-1} = \text{Pa s}$)
ρ	Density (kg m^{-3})
ρ_{opt}	Optical reflectance (-)
σ	Stefan Boltzmann constant ($5.67 \cdot 10^{-8} \text{ W m}^{-2} \text{ K}^{-4}$)

Subscripts

a	ambient
aw	artificial wall
b	backside
bw	building wall
c	convective
cf	convective front
cb	convective back
f	front
k	conductive
kf	conductive front
kb	conductive back
lam	laminar
nc	natural convection
r	radiative
rb	radiative back
rf	radiative front
tur	turbulent
v	forced convection
w	water

Acknowledgements—The authors would like to express their sincere thanks to Bodo von Moltke, who built the solar simulator, and to Leopoldo Bastos, who enabled the instrumentation to measure air velocity, and for the support of Solon AG who financed a major part of this project.

APPENDIX A

The theoretical background for the energy flows found during the experiments is presented

below. The calculation of heat fluxes by this model was carried out, and then compared to the actual measurements.

The total heat flow, q , generated by a PV-facade element could be described by:

$$q = G \cdot (1 - \rho_{\text{opt}} - \eta_{\text{PV}}) \quad (\text{A.1})$$

Reflection losses ρ_{opt} depend on the optical properties of the materials, the incidence angle and the spectrum, while photovoltaic conversion efficiency, η_{PV} , is a function of irradiance, spectrum and operating temperature. A detailed model of the optical, thermal and electrical parameters defining reflection losses, heat flow, cell temperature and performance is given by Krauter (1993) and by Krauter and Hanitsch (1996). The reflection losses ρ_{opt} for the modules used (calculated with a three-layer model, including optical dispersion and non-ideal antireflective coating) amount to 13.1%. The actual photovoltaic conversion efficiency, η_{PV} , measured at $G = 700 \text{ W m}^{-2}$ and $T_{\text{cell}} = 27^{\circ}\text{C}$, was 8.5% for a frameless PV module.

For equilibrium conditions the generated heat flow, q , has to be dissipated by conduction (q_k), convection (q_c) and irradiation (q_r) from the front (subscript f) and back surface (subscript b) of the PV module. In the case of additional thermal use (HYTIPVE), the heat-flow dissipation by the flowing water also has to be considered (q_w):

$$q = q_k + q_c + q_r + q_w \quad (\text{A.2})$$

$$q = q_{\text{kf}} + q_{\text{kb}} + q_{\text{cf}} + q_{\text{cb}} + q_{\text{rf}} + q_{\text{rb}} + q_w \quad (\text{A.3})$$

Due the type of mounting, heat flow by conduction is negligible if no insulation material is used on the backside. At the experiments that do have a backside insulation heat dissipation by convection and by radiation on the back can be neglected. For the experiment with the curtain facade, the radiation exchange between the module and the back wall is considered as a heat exchange between quasi infinite parallel plates:

$$q_{\text{rb}} = \frac{\sigma(T_{\text{b}}^4 - T_{\text{aw}}^4)}{\frac{1}{\varepsilon_{\text{b}}} + \frac{1}{\varepsilon_{\text{aw}}} - 1} \quad (\text{A.4})$$

The emittances of the materials can be found in Table 8. Doing radiation calculations, temperatures are expressed in Kelvin. Therefore, no measurements could be taken from the artificial wall, instead, the arithmetic average of back temperature and ambient temperature was used. The error obtained by setting the front and back

temperatures equal to the cell temperature was only 1.5 K (Krauter, 1993).

Therefore, the floor temperature is the same as the ambient temperature, the view factor is unity and the radiation exchange of the module front with the wall and the floor results in:

$$q_{rf} = \sigma \cdot \varepsilon_f \cdot (T_f^4 - T_{wall}^4) \quad (\text{A.5})$$

To simplify the calculations, the wall temperature was set to ambient temperature.

Therefore, the experiment with forced convection was set up symmetrically and was located relatively far away from the back wall; q_{rb} can be calculated equivalently to (A.5) using T_b and ε_b . The heat flux generated by convection of air at the front surface of the module is:

$$q_{cf} = h_{cf} \cdot (T_f - T_a) \quad (\text{A.6})$$

For natural convection, the heat transfer coefficient, h_{cf} , at a surface of a PV-facade element, with length l , could be expressed by h_{nc} , as follows (according to Merker, 1987):

$$h_{nc} = \frac{k}{l} Nu_{nc} = 0.56 \frac{k}{l} Ra^{1/4} \quad (\text{A.7})$$

$$Ra = Pr \cdot Gr = Pr \cdot \frac{g\beta l^3}{\nu^2} (T_f - T_a) \quad (\text{A.8})$$

The backside of the PV curtain facade could be modeled as an air-duct with heating from one side. For this case ($Gr > 1$), VDI (1994) gives a solution, as follows:

$$Nu = 0.61 \cdot (Pr \cdot Gr)^{1/4} = 0.61 \cdot \left(Pr \cdot \frac{g\beta(T_b - T_{aw})d^4}{\nu^2 l} \right)^{1/4} \quad (\text{A.9})$$

The properties for air required can be found in Table 7 as a function of temperature. According to VDI (1994), a reasonable value to use as a reference temperature for these properties is the average between ambient and body temperature. Further investigations on this subject were carried out by Sandberg and Moshfegh (1998).

For forced convection within a range of $0.13 \cdot 10^{-3} \text{ m s}^{-1} < v < 1.33 \cdot 10^2 \text{ m s}^{-1}$, the heat transfer coefficient for forced convection can be found (derived from VDI, 1991 and Merker, 1987) as:

$$h_v = \frac{k \cdot Nu_v}{l} = \frac{k}{l} (Nu_{lam}^2 + Nu_{tur}^2)^{1/2} \quad (\text{A.10})$$

$$Nu_{lam} = 0.664 \cdot Re^{1/2} Pr^{1/3} \quad (\text{A.11})$$

$$Nu_{tur} = \frac{0.037 Pr Re^{0.8}}{1 + 2.433 Re^{-0.1} (Pr^{2/3} - 1)} \quad (\text{A.12})$$

with:

$$Re = \frac{v \rho l}{\mu} \quad (\text{A.13})$$

In the experiment for forced convection, front and back heat transfer was about the same: $q_{cb} \approx q_{cf} = h_v (T_f - T_a)$. For air velocities $v < 1 \text{ m s}^{-1}$, heat transfer by natural convection could be more than by forced convection. In the case of a similar direction of natural and forced convection, Churchill (1977) suggested a superposition of both components:

$$h_c = \frac{k}{l} (Nu_v^3 + Nu_{nc}^3)^{1/3} \quad (\text{A.14})$$

The heat flux dissipated by the water flow \dot{m} at the last experiment is:

$$q_w = c_w \dot{m} (T_{outlet} - T_{inlet}) \quad (\text{A.15})$$

with:

$$\dot{m} = \rho_w \cdot \dot{V} \quad (\text{A.16})$$

The distributions of the heat and power fluxes of the different experiments have been calculated using the data from Tables 5–8 and using Eqs. (A.1)–(A.16). The results are presented in Table 9; the computed values fit the measurements relatively well, with maximum deviations of +5.9% and –7.9%.

Table 7. Properties of air at different temperatures (data by VDI, 1994)

Property/temperature	20°C	30°C	40°C	50°C ^a	60°C
c_p (in $\text{kJ K}^{-1} \text{kg}^{-1}$)	1.007	1.007	1.007	1.008	1.009
k (in $10^{-3} \text{ W m}^{-1} \text{ K}^{-1}$)	25.69	26.43	27.16	27.88	28.60
Pr (in –)	0.7148	0.7134	0.7122	0.7111	0.7100
β (in 10^{-3} K^{-1})	3.421	3.307	3.200	3.104	3.007
ρ (in kg m^{-3})	1.188	1.149	1.112	1.079	1.045
ν (in $10^{-6} \text{ m}^2 \text{ s}^{-1}$)	15.35	16.30	17.26	18.27	19.27
μ (in $10^6 \text{ kg m}^{-1} \text{ s}^{-1}$)	18.24	18.72	19.20	19.72	20.24

^a Values were obtained by linear interpolation.

Table 8. Thermal emittances of module and building materials (at 20–80°C)

Material	Emittance, ε	References
Aluminium (oxidized)	0.2	VDI, 1994
Glass	0.94	VDI, 1994
White paint	0.925	VDI, 1994
Building surface	0.91	Grigull and Blanke, 1989
Wood (pressboard)	0.90	Grigull and Blanke, 1989
Back cover of module (PTFE)	0.97	Grigull and Blanke, 1989

Table 9. Distribution of heat and power fluxes for different types of PV-facade elements (PVE), calculated according to Eqs. (A.1) to (A.15) using data from Tables 5–8

Energy flux	HYTIPVE flow rate $47.7 \cdot 10^{-6} \text{ m}^3 \text{ s}^{-1}$	PVE ventilated at 2 ms^{-1}	conv. PVE- air duct of 150 mm	TIPVE insulation of 125 mm
$\rho_{\text{opt}} \text{ G (in } \text{W m}^{-2}\text{)}$	92.0	92.0	92.0	92.0
$P_{\text{PV}}/A \text{ (in } \text{W m}^{-2}\text{)}$	54.1	53.3	43.8	42.3
$q_{\text{k}} \text{ (in } \text{W m}^{-2}\text{)}$	4.2	0	0	17.4
$q_{\text{rt}} \text{ (in } \text{W m}^{-2}\text{)}$	81.4	94.4	219.3	393.2
$q_{\text{rb}} \text{ (in } \text{W m}^{-2}\text{)}$	0	94.4	110.4 ^a	0
$q_{\text{ct}} \text{ (in } \text{W m}^{-2}\text{)}$	35.9	164.3	109.7	196.5
$q_{\text{cb}} \text{ (in } \text{W m}^{-2}\text{)}$	0	164.3	125.2	0
$q_{\text{w}} \text{ (in } \text{W m}^{-2}\text{)}$	379.2	0	0	0
Sum of energy fluxes	646.8	662.7	700.4	741.4
Relative difference from 700 Wm^{-2}	-7.6%	-5.3%	+0.06%	+5.9%

^a At the conventional PVE the temperature of the artificial wall was set to $T_{\text{aw}} = 0.5 (T_{\text{b}} + T_{\text{a}})$ for radiation exchange between module backside and artificial wall.

REFERENCES

- Bendel C., Rudolph U. and Viotto M. (1997) PV-Experimental-Fassade – Untersuchungsergebnisse und Kosten-reduktionspotentiale. In *Tagungsband Zwölftes Symposium Photovoltaische Sonnenenergie (Proceedings 12th Symposium on Photovoltaic Solar Energy), 26–28 February, Staffelstein, Germany*, Kleinkauf W. (Ed.), pp. 76–85, Ostbayerisches Technologie Transfer Institut e.V. (OTTI).
- Bergende T. and Løvvik O. E. (1996) Model calculations on a flat-plate solar heat collector with integrated solar cells. *Solar Energy* **55**, 453–462.
- Brinkworth B. J., Cross B. M., Marshall R. H. and Yang H. X. (1997) Thermal regulation of photovoltaic cladding. *Solar Energy* **61**, 169–178.
- Crick F. J., Wishaw A., Pearsall N., Hynes K., Shaw M., Young G. and Baker P. (1997) Photovoltaic ventilated facade: system investigation and characterisation. In *Proceedings of the 14th European Photovoltaic Solar Energy Conference, 30 June–4 July, Barcelona, Spain*, pp. 1914–1917, H. S. Stephens & Associates.
- Crick F. J., Wishaw A., Pearsall N., Hynes K., Shaw M., Young G. and Baker P. (1998) PV cladding thermal gains: experimental results from three PV cladding systems investigating the effects on the design on the operational temperature. In *Proceedings of the 2nd World Conference and exhibition on Photovoltaic Energy Conversion, 6–10 July, Vienna, Austria*, Schmid J., Ossenbrink H. A., Helm P., Ehmann H. and Dunlop E. D. (Eds.), pp. 2062–2065.
- Churchill S. W. (1977) A comprehensive correlating equation for laminar assisting, forced and free convection. *AIChE* **10**, 10–16.
- Emery K., Burdick J., Caiyem Y., Dunlavy D., Field H., Kroposki B. and Moriarty T. (1996) Temperature dependence of photovoltaic cells, modules, and systems. In *Proceedings of the 25th IEEE PV Specialists Conference, May 13–19, Washington DC, USA*, pp. 1275–1278.
- Grigull U. and Blanke W. (1989). *Thermophysikalische Stoffgrößen*, Springer, Berlin, Heidelberg, New York.
- Hänel A. and Imamura M. S. (1992) Improvement of PV array performance. In *Proceedings of the 11th E.C. Photovoltaic Conference, 12–16 October, Montreux, Switzerland*, Guimarães L., Palz W., de Reyff C., Kiess H. and Helm P. (Eds.), pp. 1088–1093.
- King D. L. and Eckert P. E. (1996) Characterizing (rating) the performance of large photovoltaic arrays for all operating conditions. In *Proceedings of the 25th IEEE PV Specialists Conference, May 13–19, Washington DC, USA*, pp. 1385–1388.
- Krauter S. (1993). *Betriebsmodell der optischen, thermischen und elektrischen Parameter von PV-Modulen*, Verlag Köster, Berlin.
- Krauter S. and Hanitsch R. (1996) Actual optical and thermal performance of PV modules. *Solar Energy Materials and Solar Cells* **41/42**, 557–574.
- Merker G. P. (1987). *Konvektive Wärmeübertragung*, Springer, Berlin, Heidelberg, New York.
- Nordmann T., Dürr M. and Fröhlich A. (1997) The 32 kW PV Installation on the Grain Silo of the Stadtmühle CMZ—the First Installation for the Zürich Solar Power Exchange. In *Proceedings of the 14th E. C. Photovoltaic Conferences, 30 June–4 July, Barcelona, Spain*, pp. 1983–1986.
- Posansky M. and Gnos S. (1994) Building integrated photovoltaic systems: examples of realised hybrid PV-power plants with specially conceived PV-modules for building integration. In *Proceedings of the 12th E.C. Photovoltaic Conference, 11–14 April, Amsterdam, The Netherlands*.
- Sandberg M. and Moshfegh B. (1998) Flow and heat transfer in the air gap behind photovoltaic panels. *Renewable and Sustainable Energy Reviews* **2**, 287–301.
- VDI (1991). *VDI Wärmeatlas*, 6th Ed., Verband Deutscher Ingenieure (Eds), VDI, Düsseldorf (Germany).
- VDI (1994). *VDI Wärmeatlas*, 7th Ed., Verband Deutscher Ingenieure (Eds), VDI, Düsseldorf (Germany).
- Wilshaw A. R., Bates J. R. and Pearsall N. M. (1996) Photovoltaic module operating temperature effects. In *Proceedings of EuroSun '96, Munich, Germany*, Goetzberger A. and Luther J. (Eds.), pp. 940–944.